

## **DETERMINING AN APPROPRIATE INITIAL VALUE OF ECCENTRICITY FOR LOW EARTH SATELLITES USING EULER METHOD**


**Rasha H. IBRAHIM**<sup>1</sup>


### **Abstract:**

The major goal of this research was to use the Euler method to determine the best starting value for eccentricity. Various heights were chosen for satellites that were affected by atmospheric drag. It was explained how to turn the position and velocity components into orbital elements. Also, Euler integration method was explained. The results indicated that the drag is deviated the satellite trajectory from a keplerian orbit. As a result, the Keplerian orbital elements alter throughout time. Additionally, the current analysis showed that Euler method could only be used for low Earth orbits between (100 and 500) km and very small eccentricity ( $e = 0.001$ ).

**Key Words:** Orbit, Orbital Elements, Satellite Perturbation, Euler Method, State Vectors.

---

 <http://dx.doi.org/10.47832/MinarCongress8-2>

<sup>1</sup>  Department of Astronomy and Space, College of Science, University of Baghdad, Baghdad, Iraq, [Rasha.Ibrahim@sc.uobaghdad.edu.iq](mailto:Rasha.Ibrahim@sc.uobaghdad.edu.iq)

## 1. Introduction:

A precise evaluation of the real orbit is necessary for perturbation to be evaluated precisely. A satellite's true orbit and keplerian orbit are separated by the perturbation [1, 2]. The atmospheric drag changes the size and shape of the orbit. The main non-conservative force that affects a satellite at low heights is one that causes friction on it, which drains energy from the orbit. Additionally, the energy reduction results in a satellite orbit degrading until it re-enters the atmosphere [3]. There are many numerical integration methods, which are used in orbit integration. In general, they are classified into two types: single step methods and multi-step methods. Both of those methods can be used as fixed step or variable step. In fixed step, the step size is constant and the integration method is carried out using this step size. On the other hand, in variable step, the step size depends on the precision of integration [4, 5]. The satellite equation is solved numerically using Euler method, but this differential equation must be transformed to a first order differential equation. By integrating the perturbed acceleration, the satellite position, velocity and orbital elements at any moments of time are computed [6].

## 2. Previous Works

The integration methods for the satellite's equation attracted the attention of numerous scholars; Roberto and Sergio studied two conventional perturbation methods for integrating satellite orbits numerically in the formulation utilizing Cartesian coordinates. They compared specifically with Encke and the variation-of-parameters (VOP) techniques [7]. Balázs and Lóránt estimated the orbit of the most modern LEO spacecraft; conventional numerical integration methods were tested. In general, the space between two discrete observed epochs is often filled using numerical integration techniques for orbit determination including Runge-Kutta, Bulirsch-Stoer, and Adams-Moulton [8]. Jeffrey *et al.* proposed an unique variable-step Gauss-Legendre implicit-Runge-Kutta (VGL-IRK) method for orbit and the spread of instability [9]. Thomas and Dimitrios focused on the accuracy evaluation of numerical integrator in the single-step and multistep techniques categories [10]. Mishra *et al.* determined the satellite's orbit includes a number of methods for measuring the motion of the satellite in terms of its position and speed [11]. Thangavel *et al.* evaluated the  $J_2$  effect and aerodynamic forces. Keeping satellites moves in relation to one another in the presence of  $J_2$  disruption to track error bounds [12]. Saneliso and Wei-Hsi created a numerical model in two dimension of a lunar-influenced Earth satellite orbit. The orbits of the satellites around the Earth were employed in the first portion of the numerical simulation [13]. Ahmed *et al.* examined the accuracy and effectiveness of numerical integration methods for solving the two-body gravitationally perturbed equation [14]. Rasha and Abdul-Rahman provided a suitable eccentricity value for satellites in Low Earth Orbit (LEO) using Runge-Kutta method. It was explained how to transform the orbital components into state vectors [15]. In the next year, Rasha and Abdul-Rahman used the fourth order Adams-Bashforth method to solve the perturbed equation of motion, it was employed in this

research to analyze the modification of orbital elements under the impact of drag [16]. Geul *et al.* calculated mathematically the satellite position and velocity over time by verified the interval orbit propagation [17].

### 3. Methodology

#### 3.1. The Satellite's State Vector

The satellite is moving in the equatorial plane with the following position and velocity [18]:

$$\left. \begin{aligned} X &= P_x x_w + Q_x y_w + W_x z_w \\ Y &= P_y x_w + Q_y y_w + W_y z_w \\ Z &= P_z x_w + Q_z y_w + W_z z_w \end{aligned} \right\} \quad (1)$$

$$\left. \begin{aligned} \dot{X} &= P_x \dot{x}_w + Q_x \dot{y}_w + W_x \dot{z}_w \\ \dot{Y} &= P_y \dot{x}_w + Q_y \dot{y}_w + W_y \dot{z}_w \\ \dot{Z} &= P_z \dot{x}_w + Q_z \dot{y}_w + W_z \dot{z}_w \end{aligned} \right\} \quad (2)$$

Where,  $P_x, P_y, P_z, Q_x, Q_y, Q_z, W_x, W_y, W_z$  are Euler angles.

$x_w, y_w, z_w, \dot{x}_w, \dot{y}_w, \dot{z}_w$  are the satellite position and velocity in the plane of the orbit can be written as the following [3]:

$$\left. \begin{aligned} x_w &= a(\cos Ec - e) \\ y_w &= a\sqrt{1 - e^2} \sin Ec \\ z_w &= 0 \end{aligned} \right\} \quad (3)$$

$$\left. \begin{aligned} \dot{x}_w &= -\frac{\sqrt{\mu a}}{r} \sin Ec \\ \dot{y}_w &= \frac{\sqrt{\mu a} (1 - e^2)}{r} \cos Ec \\ \dot{z}_w &= 0 \end{aligned} \right\} \quad (4)$$

Where:

Ec: is eccentric anomaly.

a: is semi-major axis.

e: is eccentricity.

$\mu$  : is the Earth's gravitational constant equal to  $398600 \text{ km}^3/\text{sec}^2$ .

$\theta$ : is true anomaly.

r: is the distance.

The calculation of the parameters above will explain later in orbital elements section.

### 3.2. The Satellite's Orbital Elements

The satellite has six orbital elements, which are:

- Semi-major axis is given by [19]:

$$a = \left( \frac{h^2}{\mu} \times \frac{1}{1 - e^2} \right) \quad (5)$$

Here, h is the angular momentum.

- Eccentricity can be calculated by [20]:

$$\mathbf{e} = \frac{1}{\mu} \left[ \left( |\mathbf{v}|^2 - \frac{\mu}{r} \right) \cdot \mathbf{r} - (\mathbf{r} \cdot \mathbf{v}) \cdot \mathbf{v} \right] \quad (6)$$

Where:

**r**: is the vector of the position.

**v**: is the vector of the velocity.

r: is the distance.

- Inclination is defined as follows [19]:

$$\cos i = h_z/h \quad (7)$$

Where:

$h_z = x_w \dot{y}_w - y_w \dot{x}_w$ , which is the angular momentum in Z-direction.

h: is the angular momentum magnitude.

- Longitude of ascending node is [19]:

$$\cos \Omega = N_x/N \quad (8)$$

Here,  $N_x$  is the line of node vector in X-direction, equal to  $\mathbf{k}_x \times \mathbf{h}_x$ .

N: is the magnitude of the line of node.

- Argument of perigee is applied as [19]:

$$\cos \omega = \mathbf{N} \cdot \mathbf{e} / N \cdot e \quad (9)$$

Where:

**e**: is eccentricity vector.

- True anomaly are calculated by [19]:

$$\cos \theta = \mathbf{e} \cdot \mathbf{r} / e \cdot r \quad (10)$$

### 3.3. The Perturbed Acceleration

This type of perturbation is represented as below [3]:

$$\ddot{\mathbf{r}}_{\text{Drag}} = -\frac{1}{2} C_D \frac{A}{M} \rho \frac{\mathbf{v}_r}{v_r} \quad (11)$$

Where:

$C_D$ : is drag's parameter.

$A/M$ : is the ratio of the satellite's area to its mass.

$\mathbf{v}_r$ : is the satellite's relative velocity vector.

$v_r$ : is the satellite's relative velocity magnitude.

$\rho$ : is the density of the atmosphere, this density is computed by NRLMSISE-00.

The equation of motion without perturbation is [3]:

$$\ddot{\mathbf{r}} = -\frac{\mu}{r^3} \mathbf{r} \quad (12)$$

Adding equation (11) to (12), the final representation of the equation of motion (under the influence of atmospheric drag) is [20]:

$$\ddot{\mathbf{r}}_P = -\frac{\mu}{r^3} \mathbf{r} + \ddot{\mathbf{r}}_{\text{Drag}} \quad (13)$$

**Table (1): Give a representation of the parameter's initial values utilized in the program [3, 4, 15, 16, 21].**

Parameter	Case (1)	Case (2)	Case (3)	Case (4)
$h_p$ (km)	250	250	500	900
$a$ (km)	6625	6685	6885	7385.53
$e$	0.001	0.01	0.001	0.001
$i$ (deg)	70	70	70	70
$\Omega$ , (deg)	50	50	50	50
$\omega$ (deg)	100	100	100	100
$M_e$ (deg)	0	0	0	0
$E_c$ (deg)	0	0	0	0
$\theta$ (deg)	0	0	0	0
$C_R$	2.2	2.2	2.2	2.2
$C_D$	1.3	1.3	1.3	1.3
$A / M$ (m <sup>2</sup> /kg)	0.0052	0.0052	0.0052	0.0052
$h$	5.4393	5.4393	5.6855	6.1886

### 3.4. Euler Method

The new satellite's position and velocity components are computed as [3, 6]:

$$X_f = X_i + \frac{h}{6} (A_X)$$

$$\left. \begin{aligned} Y_f &= Y_i + \frac{h}{6} (A_Y) \\ Z_f &= Z_i + \frac{h}{6} (A_Z) \end{aligned} \right\} \quad (14)$$

$$\dot{X}_f = \dot{X}_i + \frac{h}{6} (B_X)$$

$$\left. \begin{aligned} \dot{Y}_f &= \dot{Y}_i + \frac{h}{6} (B_Y) \\ \dot{Z}_f &= \dot{Z}_i + \frac{h}{6} (B_Z) \end{aligned} \right\} \quad (15)$$

Where:

$X_i, Y_i, Z_i$ : is the initial position in X, Y, and Z.

$X_f, Y_f, Z_f$ : is the final position in X, Y, and Z.

$\dot{X}_i, \dot{Y}_i, \dot{Z}_i$ : is the initial velocity in X, Y, and Z.

$\dot{X}_f, \dot{Y}_f, \dot{Z}_f$ : is the final velocity in X, Y, and Z.

The six parameters  $A_X, A_Y, A_Z, B_X, B_Y, B_Z$  are computed as following:

$$A_X = \dot{X}_i, A_Y = \dot{Y}_i, A_Z = \dot{Z}_i$$

$$B_X = \ddot{r}_{X0}, B_Y = \ddot{r}_{Y0}, B_Z = \ddot{r}_{Z0}$$

Where:

$\ddot{r}_{X0}, \ddot{r}_{Y0}, \ddot{r}_{Z0}$  is initial perturbed acceleration in X, Y, and Z direction.

h: is the integration step size.

## 4. Results and Discussion

The evaluation for six orbital elements was utilized to explain the satellite's orbit under the influence of atmospheric drag. This analysis was made by using different cases, as presented in table (1). Figure (1) demonstrated how the drag affected the semi-major axis. It was observed that the value of semi-major axis for case (1) is monotonically dropping with time. In case 2, this element has a fast decreasing with respect to the number of days, also after the fourth day, it has a constant appearance. In case 3, semi-major axis was linearly decreasing with time, but in case 4, it was linearly increasing, so it was observed that the small value of eccentricity is more affected by drag than other heights.

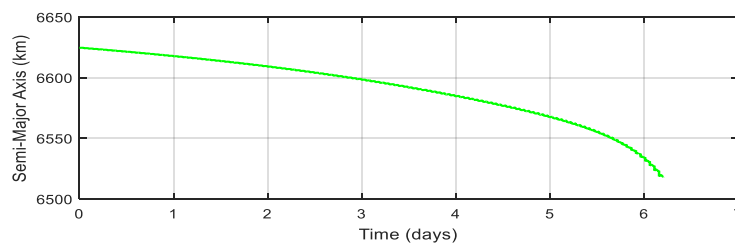
In ideal conditions, the appearance of eccentricity was constant with time, but in figure (2), case 1, it reduced gradually from (0.0001 to 0.00098). The performance of eccentricity in case (2) was also decreasing then be constant with time. In case (3), it observed that the value of eccentricity is dropping with time like semi-major axis. This element in case (4), has a slow growing relationship with the number of days.

Figure (3) depicted the influence of eccentricity and the height on inclination angle. In case 1, this element decreases a little as the time passes and then decreases very fast until reaches the value  $69.973^\circ$ . In case 2, it has a sharp dropping after the second day, this element drops very fast until reaches to a constant value  $69.99652^\circ$ . In case (3) and (4), inclination was linearly reducing with time.

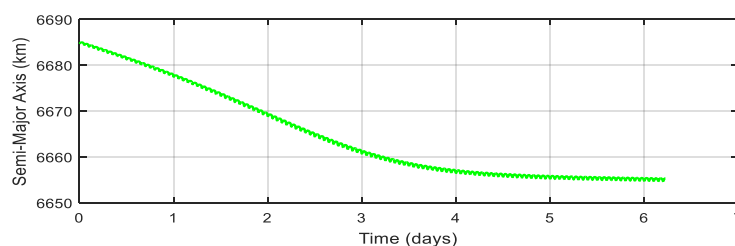
Figure (4) illustrated right ascension of ascending node, which has a value between  $(50-50.007)^\circ$  in case 1. Therefore, the drag moved away this element from its desired value. In case (2), right ascension of ascending node has a hump, then decreasing with time. This element in case (3) and (4), was linearly increasing as the time passes. The ideal value of this element was  $50^\circ$ , but with the assumption of atmospheric drag, it reaches to  $50.0001^\circ$  on the sixth day.

The influence of atmospheric drag on argument of perigee for all cases was linearly growing with time. Also, this perturbation makes this element deflects from its ideal value, as in figure (5).

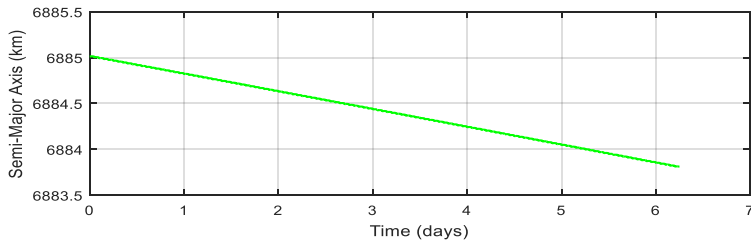
Finally, true anomaly increases from 0 to  $360^\circ$  for one period. It has a toothed appearance in every case and for seven days, as shown in figure (6).



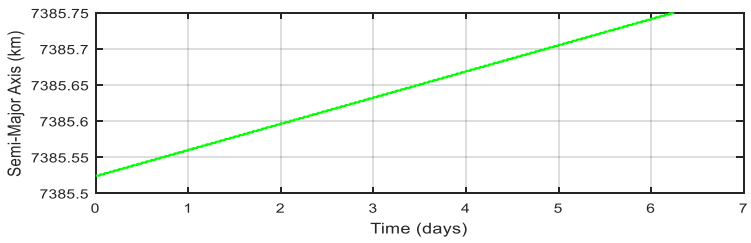
**Case (1)**



**Case (2)**

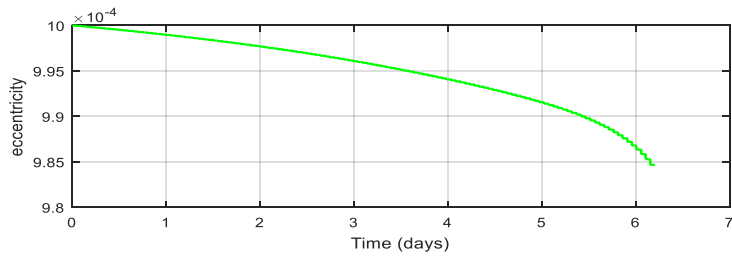


**Case (3)**

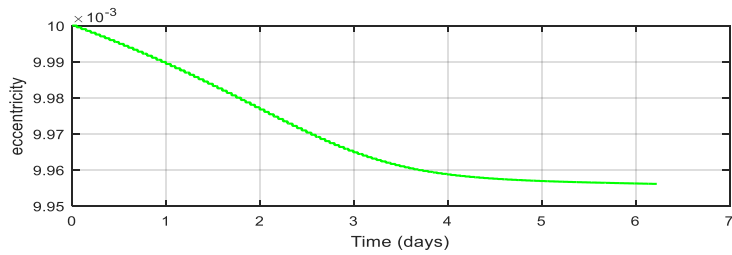


**Case (4)**

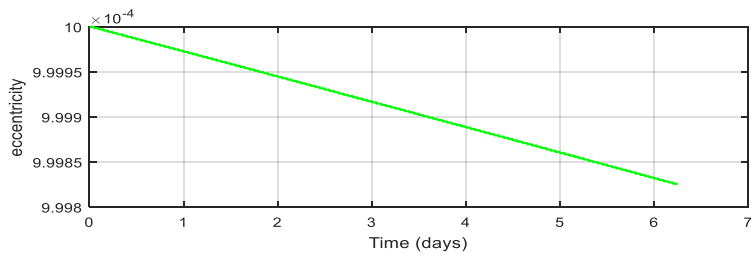
**Figure (1): Semi-major axis with different cases.**



**Case (1)**

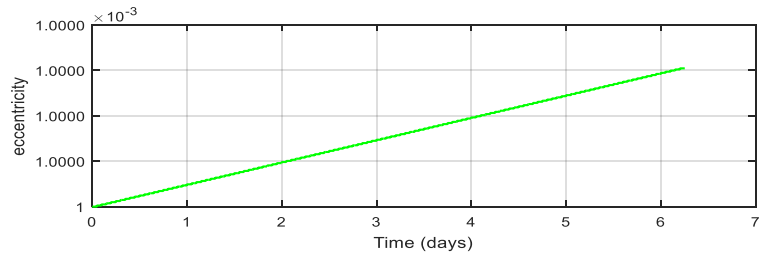


**Case (2)**



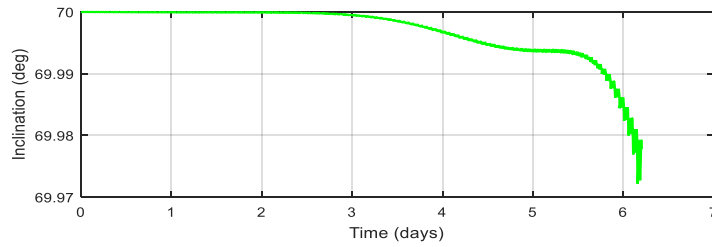
**Case (3)**



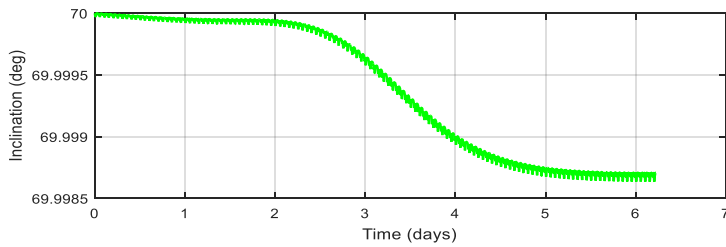


**Case (4)**

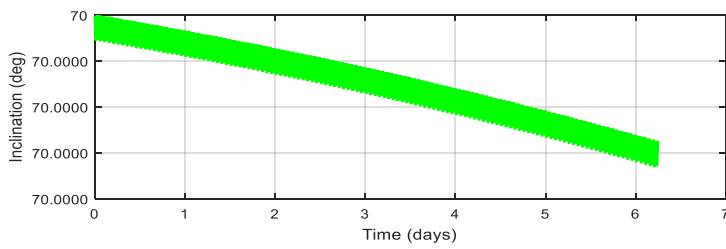
**Figure (2): Eccentricity with various cases.**



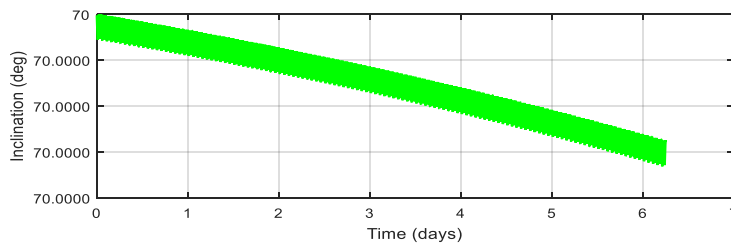
**Case (1)**



**Case (2)**

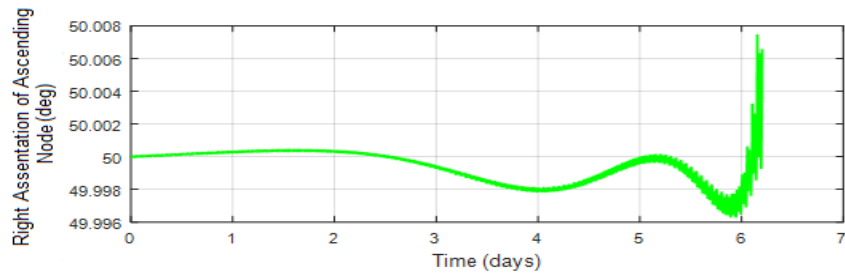


**Case (3)**

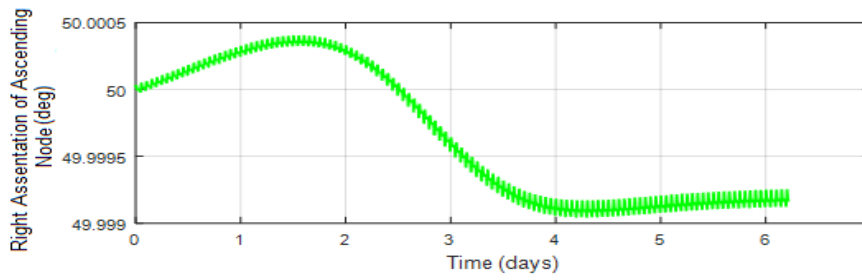


**Case (4)**

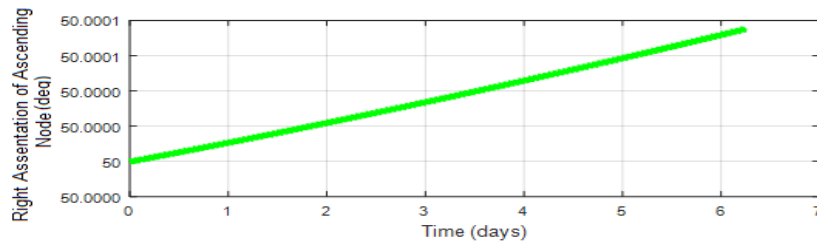
**Figure (3): Inclination with diverse cases.**



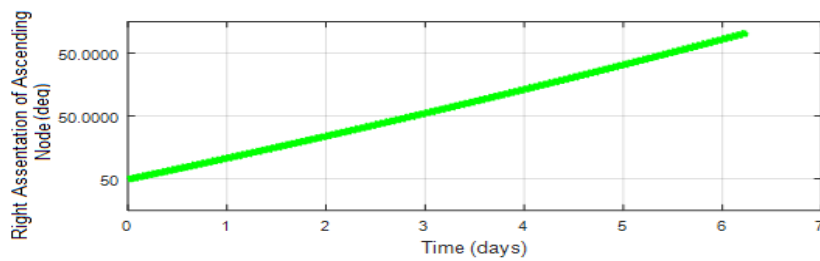
**Case (1)**



**Case (2)**

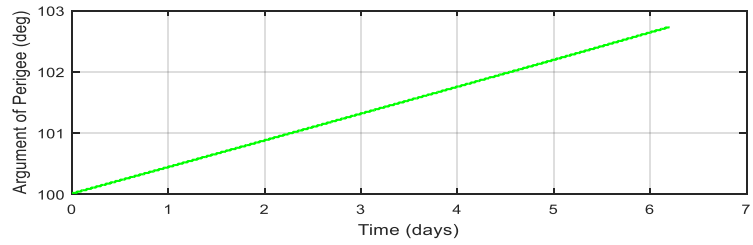


**Case (3)**

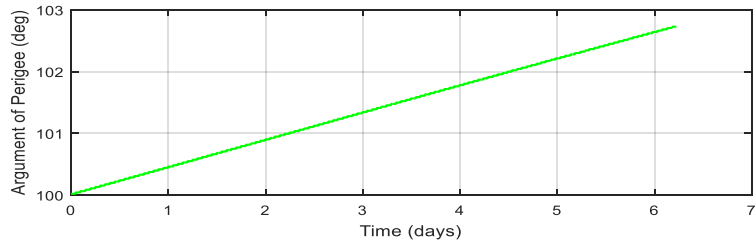


**Case (4)**

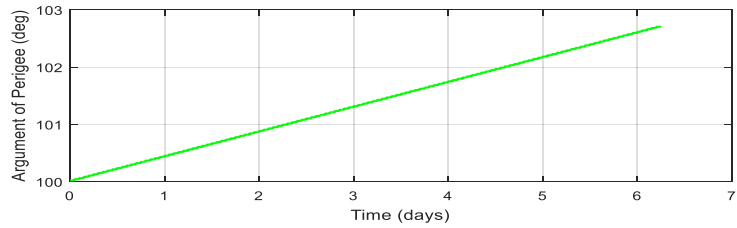
**Figure (4): Right assentation of ascending node with different cases.**



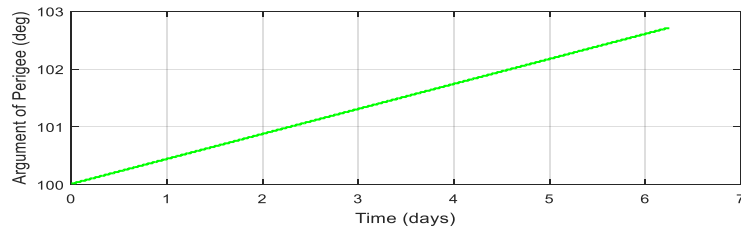
**Case (1)**



**Case (2)**

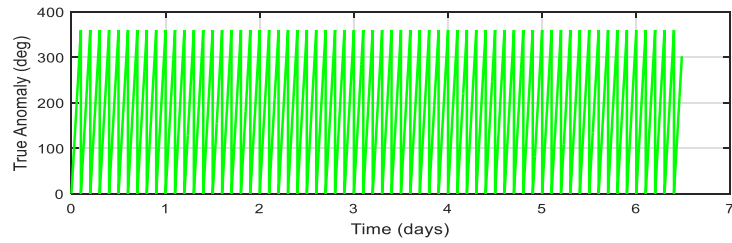
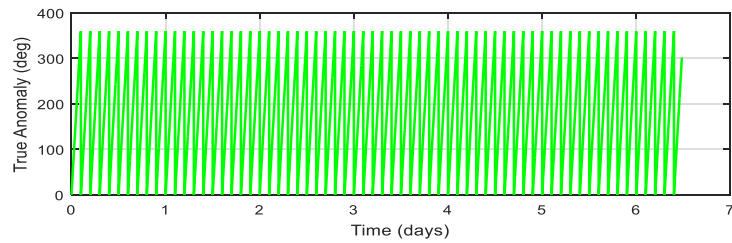
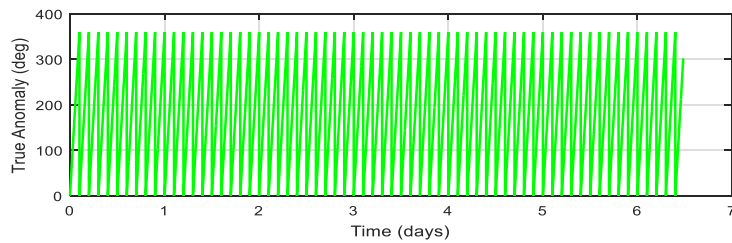
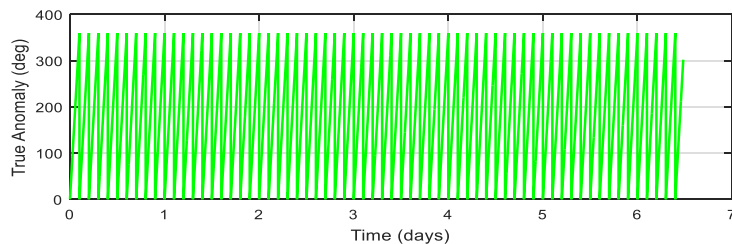


**Case (3)**



**Case (4)**

**Figure (5): Argument of perigee with various cases.**

**Case (1)****Case (2)****Case (3)****Case (4)****Figure (6): True anomaly with different cases.**

## 5. Conclusions

1. From the appearance of the semi-major axis and eccentricity, Euler method was applicable for very small values of eccentricity, which was equal to or smaller than 0.0001 and very low heights started from (100-500) km.
2. The directional elements, inclination, longitude of the ascending node, argument of perigee, and true anomaly at heights greater than 500 km, are unaffected by eccentricity regardless of its value.
3. Eccentricity and semi-major axis were rapidly decreased, particularly in recent days.

4. The results demonstrated a good agreement with a number of previously published researches that used the Runge-Kutta method of the fourth order [15, 16, 22, 23] and Adams-Bashforth Method of the fourth order [24].

## References

1. M. Eshagh and Najafi Alamdari M, Perturbations in Orbital Elements of a Low Earth Orbiting Satellite, *Journal of the Earth & Space Physics*.**33** 1 (2007)1-12.
2. Pelton, J.N., **2012**. Satellite Communications. Chapter 2: Orbits, Services and Systems. Springer Briefs in Space Development.
3. Montenbruck, O. and Gill, E. **2001**. Satellite Orbits Models Methods and Applications. Second Edition, Springer-Verlag Berlin Heidelberg, Printed in Germany.
4. Richard, H. Battin and. **1999**. An Introduction to the Mathematics and Methods of Astrodynamics, Revised Edition. AIAA Education Series.
5. Es-hagh, M. **2005**. Step Variable Numerical Orbit Integration of a Low Earth Orbiting Satellite. *Journal of the Earth and Space Physics*, Vol. 31, No. 1, pp. 1-12.
6. Bate, R., Mueller, D. and White, J., **1971**. Fundamental of Astrodynamics. Dover publications, Inc. New York.
7. Roberto Barriola and Sergio Serrano. 2008. Performance of perturbation methods on orbit prediction. *Mathematical and Computer Modelling*. 48: 594–600
8. Balázs Somodi and Lóránt Földvály. **2011**. Application of numerical integration techniques for orbit determination of state-of-the-art LEO satellites. *Periodica Polytechnica Civil Engineering*. 55(2): 99–106.
9. Jeffrey M. Aristoff, Joshua T. Horwood, Aubrey B. Poore. **2013**. Orbit and uncertainty propagation: a comparison of Gauss–Legendre-, Dormand–Prince-, and Chebyshev–Picard-based approaches. *Celest Mech Dyn Astr*  
DOI 10.1007/s10569-013-9522-7.
10. Thomas, D. P. and Dimitrios T. **2016**. Assessment of numerical integration methods in the context of low Earth orbits and inter-satellite observation analysis. *Acta Geod Geophys*. **51**:619–641
11. Mishra, S. Singh, G. Singh, M. and Gaba, G. **2017**. ISDA Based Precise Orbit Determination Technique for Medium Earth Orbit Satellites", *Pertanika Journal Science and Technology*, Vol. 25, No. 4, pp. 1357-1368.
12. Thangavel, S., Santhanakrishnan, R., and Lakshmi, S. **2018**. Study the Influence of Atmospheric Drag and J2 Effect in a Close-proximity Operation at LEO. *International Journal of Engineering & Technology*. 7(4.36):403-408.
13. Saneliso Vuyo Makhanya, Wei-Hsi Liao. **2019**. Numerical Model of Perturbated Earth's Satellite Orbit. *International Journal of Applied Mathematics and Theoretical Physics*. Vol. 5, No. 1, pp. 1-14. doi: 10.11648/j.ijamtp.20190501.11.
14. Ahmed M. Atallah, Robyn M. Woollands, Tarek A. Elgohary, John L. Junkins. **2019**. Accuracy and Efficiency Comparison of Six Numerical Integrators for Propagating Perturbed Orbits. *The Journal of the Astronautical Sciences*. doi.org/10.1007/s40295-019-00167-2.

15. Rasha H. Ibrahim and Abdul-Rahman H. Saleh. **2020**. Determination the optimum orbit for low Earth satellites by changing the Eccentricity. *Journal of Physics: Conference Series*. **1530**(012127).
16. Rasha, H. Ibrahim and Abdul-Rahman, H. Saleh. **2021**. Increasing the Accuracy of Orbital Elements for a Satellite in a Low Earth Orbit under the Influence of Atmospheric Drag Using Adams-Bashforth Method. *Iraqi Journal of Science*. Special Issue (2):81-90.
17. Geul, J., Mooij, E., Noomen, R. **2021**. Verified regularized interval orbit propagation. *Journal of Guidance, Control, and Dynamics*, 44(4), 719-731. <https://doi.org/10.2514/1.G004947>
18. Rasha, H. and Abdul-Rahman, H. **2019**. Re-Evaluation Solution Methods for Kepler's Equation of an Elliptical Orbit. *Iraqi Journal of Science*. **60**(10): 2269-2279.
19. Ahmed, H., Mohammed, K., El-Kaber, H., Tajjeeddine, R., and Mohamed, S. **2017**. Perturbation Effects in Orbital Elements of CubeSat. 3rd International Conference on Advanced Technologies for Signal and Image Processing Morocco.
20. Ulrich, W. **2019**. *Astronautics: The Physics of Space Flight*. Third Edition. Springer.
21. Seeber, G. **2003**. *Satellite Geodesy*. Second Edition. completely revised and extended edition. Walter de Gruyter. Berlin. NY.
22. Mohammed, A. and Abdul-Rahman, H. **2018**. Evaluation of Optimal Initial Conditions for Orbital Elements of Satellite. *Science Intentional (Lahore)*. **30**(5):785-796.
23. Rasha, H. and Abdul-Rahman H. **2020**. Improvement of the Accuracy of the Perturbed Orbital Elements for LEO Satellite by Improving 4th Order Runge-Kutta's Method. *Indian Journal of Science and Technology*, Vol.13, No.4, pp. 1-13.
24. Rasha H. Ibrahim, and Abdul-Rahman H. Saleh. **2020**. A comparison between Runge-Kutta and Adams-Bashforth methods for determining the stability of the satellite's orbit. AIP Conference Proceedings 2290, 050002. <https://doi.org/10.1063/5.0027420>